Identifying the Dominant Electrochemical Reaction in Electrochemical Impedance Spectroscopy

Negar Moradighadi, Srdjan Nesic, Bernard Tribollet

▶ **To cite this version:**

Negar Moradighadi, Srdjan Nesic, Bernard Tribollet. Identifying the Dominant Electrochemical Reaction in Electrochemical Impedance Spectroscopy. Electrochimica Acta, 2021, 400, pp.139460. 10.1016/j.electacta.2021.139460 . hal-03403910

HAL Id: hal-03403910
https://hal.science/hal-03403910v1

Submitted on 26 Oct 2021

HAL is a multi-disciplinary open access archive for the deposit and dissemination of scientific research documents, whether they are published or not. The documents may come from teaching and research institutions in France or abroad, or from public or private research centers.

L'archive ouverte pluridisciplinaire **HAL**, est destinée au dépôt et à la diffusion de documents scientifiques de niveau recherche, publiés ou non, émanant des établissements d'enseignement et de recherche français ou étrangers, des laboratoires publics ou privés.

Journal Pre-proof

Identifying the Dominant Electrochemical Reaction in Electrochemical Impedance Spectroscopy

Negar Moradighadi [a,*], Srdjan Nesic [a], Bernard Tribollet [b]

[a] Institute for Corrosion and Multiphase Technology, Ohio University, Athens, OH, USA

[b] Laboratoire Interfaces et Systèmes Electrochimiques (LISE), Sorbonne Université, Paris, France

[*] Corresponding author: E-mail address: nm867515@ohio.edu (N. Moradighadi)

Abstract

Electrochemical Impedance Spectroscopy (EIS) is frequently used for the study of electrochemical reactions and associated mechanisms and phenomena. To study a specific reaction, it is important to choose the DC potential at which the measured impedance data carries information mostly related to that specific reaction. One of the first questions asked was: at different potentials, which reaction contributes most to the recorded impedance spectra, cathodic or anodic? For example, at the corrosion potential where the cathodic current density is equal to the anodic current density, does the impedance data carry information about the two reactions equally? The following study is the development of a methodology that is essential as the first step for analysis of the impedance data related to an electrochemical reaction. This methodology consists of a new model that predicts which reaction is dominant to the measured impedance at any specific potential. The experimental results provided confirm the validity of the model.

Keywords: electrochemical impedance spectroscopy, dominant electrochemical reaction, DC potential, corrosion, polarization resistance

Journal Pre-proof

Journal Pre-proof

1. Introduction

EIS is an electrochemical technique that can be applied to study electrochemical mechanisms of reactions underlying corrosion, evaluate coating performance, characterize battery and fuel cell performance, etc.[1–12]. EIS can provide a wealth of information about the electrochemical reactions and surface phenomena occurring, based on analysis of the impedance response of the system. The term *impedance* is defined as "the effective resistance of an electric circuit or component to alternating current, arising from the combined effects of ohmic resistance and reactance"[13]. In other words, impedance measurements include the estimation of both the *ohmic resistance* to a flow of current and resistance to a change in current, called *reactance* that arises from the effect of inductance and/or capacitance [1]. In EIS measurements, a small amplitude, alternating signal (current or potential) is applied at different frequencies to probe the impedance characteristics of a system being studied, in our case corrosion.

In the field of corrosion, it has been common practice to use the so called *direct current* (DC) techniques to study the mechanisms of the electrochemical corrosion reactions; for some recent examples from aqueous CO_2 corrosion of mild steel, see Kahyarian et al. [14]. Usually, the DC techniques involve a rather slow change in potential and monitoring of the resulting steady state current response, such as done for example in potentiodynamic polarization methods. As an example, Figure 1a shows the results of two separate potentiodynamic polarization sweeps (cathodic and anodic) conducted on mild steel in an aqueous CO_2 solution. Both potential sweeps were initiated at the open circuit potential (OCP), and then the potential was swept at the low rate of 0.125 mV s^{-1} in the cathodic and then anodic direction. At more positive potentials than the OCP, the measured steady state current density originates predominantly from the anodic reaction – in this case oxidation of iron– and therefore carries information mainly about the rate

of this reaction. Similarly, at potentials more negative than the OCP, the measured steady state current density carries information mostly about the rate of cathodic reactions in this case evolution of hydrogen via reduction of H^+ ions and water molecules.

But does that also mean that the analysis of the impedance obtained by EIS should follow the same logic, that is: at potentials more positive than OCP, the impedance of the anodic reaction is dominating, while at more negative potentials it is the impedance of the cathodic reaction that dominates. If so, at the OCP, where the rates of the anodic and cathodic reactions are equal, do the EIS measurements detect an even contribution of both reactions to the measured impedance (see the example in Figure 1b)? The answer to this question is the main objective of the present paper. Restated more generally: before conducting EIS measurements, it is important to estimate what fraction of the impedance recorded at any given potential is contributed by one reaction or the other. In the present paper, a methodology is introduced to estimate the dominant electrochemical reaction contributing to the measured impedance at any given potential. It is the hope that the described method will help researchers better select experimental conditions, so that the collected impedance spectra carry sufficient information about the electrochemical reactions of interest. In order to demonstrate the new methodology, an experimental study was first presented, where potentiodynamic sweep were collected followed by EIS measurements conducted at different DC potentials.

Journal Pre-proof

2. Experimental

Experiments were performed in a standard 1 L, three-electrode glass cell consisting of a rotating disk working electrode (RDE), a graphite rod counter electrode and an external saturated Ag/AgCl reference electrode, connected to the solution via a salt bridge and a Luggin capillary. The experimental apparatus is shown in Figure 2. The test solution was continuously sparged

with CO_2 gas during and two hours before the initiation of the experiments, to saturate the solution and remove the dissolved O_2 (concentration levels below 10 ppb are readily achieved). The pH of the test solution was adjusted to pH 4.0 using a dilute NaOH solution. The working electrode was made from API[1] 5 L X65 mild steel (composition provided in Table 1) in the shape of a 5 mm diameter disk, which was polished by using silicon carbide papers (up to 1000 grit) and finally mirror finished using diamond suspension liquids (down to 0.25 μm). Mirror finishing was done to minimize formation of gas bubbles on the surface of the RDE during polarization and improve reproducibility of measurements. Following the surface preparation, the sample was cleaned with isopropyl alcohol in an ultrasonic bath and then dried with a N_2 gas stream. Before each polarization sweep and EIS measurements, OCP was monitored for 20-30 minutes to achieve a stable value (drift in the OCP < +/- 0.1 mV min^{-1}). After obtaining a stable OCP, the cathodic polarization sweep was conducted by polarizing the RDE from OCP to OCP – 350 mV using a scan rate of 0.125 mV s^{-1}. Following the cathodic polarization sweep, EIS measurements were performed in succession at different DC potentials, starting from OCP and stepping the DC potential by –50 mV, down to –300 mV more negative than OCP. For the measurements done at potentials more positive than OCP, an EIS measurement was performed only at OCP + 50 mV and finally, a full anodic polarization sweep was conducted from OCP to OCP + 100 mV. The summary of the test conditions for the experiments is shown in Table 2.

[1] American Petroleum Institute (API), 1220 L St. NW, Washington, DC, 20005.

3. Results and discussion

3.1. Potentiodynamic sweep and the model

In corrosion of mild steel in acidic aqueous solutions, it is known that the main anodic reaction is the oxidation of iron (Reaction (1)) and the main cathodic reaction is the reduction of hydrogen ions (Reaction (2)). At the very negative potentials, reduction of water (Reaction (3)) occurs as well.

Dissolution of iron $$Fe \rightleftharpoons Fe^{2+} + 2e^- \quad (1)$$

Reduction of hydrogen ion $$H^+ + e^- \rightleftharpoons \frac{1}{2}H_2 \quad (2)$$

Reduction of water $$H_2O + e^- \rightleftharpoons \frac{1}{2}H_2 + OH^- \quad (3)$$

Reaction (1) shows the general reaction for the iron dissolution which involves 3 consecutive steps shown in (Reactions (4)-(6))[15].

$$Fe + OH^- \rightleftharpoons (FeOH)_{ads} + e^- \quad (4)$$

$$(FeOH)_{ads} \xrightarrow{rds} (FeOH)^+ + e^- \quad (5)$$

$$(FeOH)^+ + H^+ \rightleftharpoons Fe^{2+} + H_2O \quad (6)$$

The measured potentiodynamic sweep are shown in Figure 3. In order to deconvolute the data shown there and extract those pertaining to individual electrochemical reactions, shown above, a simple mechanistic model was constructed using the kinetic equations of each electrochemical reactions (Equations (7)-(13)) with the calculated results shown in Figure 4 [15–19]. In the model, it was assumed that the iron dissolution is under pure charge transfer control and Equations (7) was use for modeling of this reaction which is approximately valid on a limited

potential range close to OCP. Moreover, it was assumed that the water reduction is under pure charge transfer control (Equation (13)) while the reduction of hydrogen ion is under charge transfer control at more positive potentials and under mass transfer and chemical reactions control at more negative potentials (Equations (8)-(12)).

Iron dissolution - charge transfer current density:

$$i_{ct,Fe} = i_{0,Fe} e^{\left(\frac{1.5F\eta}{RT}\right)} \quad (7) \quad [15–17]$$

Hydrogen ion reduction - charge transfer controlled current density:

$$i_{ct,H^+} = i_{0,H^+} e^{\left(\frac{-0.5F\eta}{RT}\right)} \quad (8) \quad [16,17]$$

Hydrogen ion reduction - mass transfer and chemical reaction limiting current density:

$$i_{lim,H^+} = 0.62F{D_{H^+}}^{2/3}\omega^{1/2}\nu^{-1/6}C_{H^+} + \frac{FD_{H^+}(C_{CO_2} + C_{H^+})}{\delta_d + \frac{\delta_r}{K_{hy,CO_2}}} \quad (9) \quad [17,19]$$

Diffusion layer thickness:

$$\delta_d = 1.61{D_{H^+}}^{1/3}\omega^{-1/2}\nu^{1/6} \quad (10) \quad [17]$$

Reaction layer thickness:

$$\delta_r = \left(\frac{D_{H^+}}{\left(k_{f,hy,CO_2,} + k_{b,hy,CO_2}\right)}\right)^{1/2} \quad (11) \quad [17]$$

Hydrogen ion reduction - total current density:

$$\frac{1}{i_{H^+}} = \frac{1}{i_{ch,H^+}} + \frac{1}{i_{lim,H^+}} \quad (12) \quad [16–18]$$

Water reduction-charge transfer controlled current density:

$$i_{ct,H_2O} = i_{0,H_2O} e^{\left(\frac{-0.5F\eta}{RT}\right)} \quad (13) \quad [16,17]$$

Summing the current densities for the three reactions gives us the overall potentiodynamic sweep, shown in Figure 4. The good fit between the experimental results and the modeled potentiodynamic sweep is shown in Figure 4. The outcome of this exercise showed that at OCP, the cathodic reaction is dominated by hydrogen ion reduction, which is under mixed charge transfer, mass transfer and chemical reactions control, as shown in Figure 4. Therefore, the corrosion current density (5.1 A m^{-2}), is close in magnitude to the limiting current density (6.7 A m^{-2}).

3.2. Identifying the dominant electrochemical reaction

Figure 4 shows the individual electrochemical reactions. Using Equation (14), we can calculate the percent contributions of individual electrochemical reaction to the total current density obtained at different potentials what is shown as a bar graph (Figure 5). At OCP + 50 mV, 88.8%. of the measured current density was related to the oxidation of iron. Conversely, at OCP – 50 mV, 86.8% of the measured current density was associated with the H^+ reduction. As the potential becomes more negative than OCP, the contribution of the current density originating from H^+ reduction to the total current density increases, and at the same time the water reduction contribution grows. As indicated in Figure 4, at very negative potentials the cathodic reaction is dominated by the water reduction reaction (not shown in Figure 5).

$$\text{Contribution of current density of reaction j} = \frac{i_j}{(i_{ct,Fe} + i_{H^+} + i_{ct,H_2O})} \times 100 \quad (14)$$

The deconvoluted data shown in Figure 4, can also be used to estimate the contribution of the individual reactions to the overall impedance that would be measured at different DC potentials.

Given that the value of impedance includes both the ohmic resistance and the reactance, only the ohmic resistance (real part of the impedance) can be calculated from the steady state data shown in Figure 4. As the mass transfer and chemical reactions (that give rise to the imaginary part of the overall impedance) and the charge transfer reactions (manifested as the real part of the overall impedance) are linked in an electrochemical process such as corrosion, we can argue that estimating the real part of the impedance gives us a reasonable estimate of the relative magnitude of the overall impedance [20].

We can now use the potentiodynamic sweep data, in order to estimate the real part of the impedance at any potential (which we will call here the *polarization resistance*, R_p), by calculating the first derivative of the current density-potential curve by using Equation (15), for each individual electrochemical reaction, shown in Figure 4.

$$R_p = \frac{\Delta V}{\Delta I} \qquad (15)$$

The results are plotted in Figure 6.

The line representing the anodic reaction in Figure 6 shows an increase in $R_{p,Fe}$ as potential becomes more negative, while for the cathodic reactions the polarization resistance decreases. However, as the limiting current density range for the H^+ reduction reaction is approached, the R_{p,H^+} for this reaction reverses course and starts to increase, as shown in Figure 6. This is because it becomes harder to change the rate of this reaction by polarization as it gets closer to the limiting current density which is controlled by slow mass transfer and homogenous chemical reaction rates. The R_{p,H_2O} keeps getting smaller at more negative potential across the whole range of potentials.

Journal Pre-proof

Using an electrical circuit analog model of this electrochemical process, where resistances arranged in parallel represent individual electrochemical reactions, the overall polarization resistance $R_{p,overall}$ can be calculated by using Equation (16). It shows that the overall polarization resistance is dominated by the smallest of the individual polarization resistances. In other words, the reaction/process with the smallest polarization resistance will be the dominant one. The overall polarization resistance for the 3 reactions is shown as the thick black line in Figure 6.

$$\frac{1}{R_{p,overall}} = \frac{1}{R_{p,Fe}} + \frac{1}{R_{p,H^+}} + \frac{1}{R_{p,H_2O}} \quad (16)$$

It is shown in Figure 6 that at more positive potentials the overall polarization resistance is dominated by the anodic reaction, given that the Fe oxidation reaction has the smallest polarization resistance in this range. In the mid-range of potentials, the contribution of H^+ reduction (which is under mass transfer control) has the largest influence on the $R_{p,overall}$. Finally, at the more negative range of potentials, the R_{p,H_2O} dominates (being the smallest of the three). Even if this behavior is qualitatively similar to the changes seen in the current density, shown in Figure 4, the two do not align entirely.

The same information is represented in Figure 7, where using Equation (17) the contributions of the three reactions to the polarization admittance ($1/R_p$) are calculated and explicitly shown at different potentials. Now, the contributions of individual reactions to the measured current density (shown in Figure 5) can be directly compared the contributions to the overall polarization admittance (shown in Figure 7) at the same potentials.

$$\text{Contribution of admittance of reaction j} = \frac{R_{p,overall}}{R_j} \times 100 \quad (17)$$

- At OCP + 50 mV, where 88.8% of the measured current density comes from the anodic reaction, the overall polarization resistance is also dominated by the same reaction. At this potential, the $R_{p,Fe}$ is much smaller than it is for the other reactions and represents 96.8% of the overall polarization admittance ($1/R_{p,overall}$). Thus, both the measured current density and the measured polarization resistance carry the information about the same reaction: Fe oxidation.
- At the OCP, the anodic and cathodic current densities are balanced (equal) and no current is flowing in the external circuit and the rates of the individual reactions cannot be assessed directly. However, at the OCP, the measured polarization resistance is still dominated by the $R_{p,Fe}$: polarization resistance for this reaction is about 4 times smaller than that for R_{p,H^+} and orders of magnitude smaller than R_{p,H_2O}. Thus, at OCP, the polarization resistance carries information mostly about Fe oxidation: polarization admittance of this reaction is 87.6% of the overall polarization admittance.
- At OCP – 50 mV, the contribution of the $R_{p,Fe}$ to the overall polarization resistance is still dominant. The polarization admittance of this reaction is 69.7% of the overall polarization admittance, while at the same time the current density is dominated by the H^+ reduction reaction (which contributes 86.8% to the measured current density). Therefore, while at this potential, the current density mostly carries information about the H^+ reduction, the polarization resistance gives us information mostly about Fe oxidation.
- At OCP – 100 mV, the $R_{p,Fe} \approx R_{p,H^+}$, while the R_{p,H_2O} is still orders of magnitude higher. At the same time 97.6 % of the measured current density comes from the cathodic reactions (mostly H^+ reduction). Again, the measured current density mostly carries information about the H^+ reduction reaction, while the measured polarization resistance

Journal Pre-proof

gives us mixed information, contributed approximately equally by both Fe oxidation and H^+ reduction.

- At OCP – 150 mV, the R_{p,H^+} is approximately half of the $R_{p,Fe}$, which is again about half of R_{p,H_2O}. At the same time, 99.6% of the measured current density comes from the cathodic reactions (with 99.1% of that contributed by H^+ reduction). Therefore, the current density carries information about the H^+ reduction, while the polarization resistance gives us mixed information dominated by the cathodic reactions: mostly H^+ reduction (polarization admittance of H^+ reduction is 59.5% of the overall polarization admittance).
- At OCP – 200 mV, 99.9% of the current density comes from the cathodic reaction (98.6% of that from H^+ reduction). At the same time, the $R_{p,Fe}$ is about 15 times higher than the ones for the R_{p,H^+} and R_{p,H_2O}. So, the current density carries information about the H^+ reduction, while the overall polarization resistance gives us mixed information mostly about the cathodic reactions contributed more by H_2O reduction and less by H^+ reduction; polarization admittance of H_2O reduction is 60.2% of the overall polarization admittance.
- At OCP – 250 mV, 99.99% of the current density comes from the cathodic reactions (with 96.6% of that from H^+ reduction) while the overall polarization resistance is dominated by R_{p,H_2O} which is an order of magnitude lower than R_{p,H^+} and two orders of magnitude lower than $R_{p,Fe}$. In this case the current density carries information about H^+ reduction, while the measured polarization resistance gives us information predominantly about H_2O reduction: polarization admittance of H_2O reduction is 91.6% of the overall polarization admittance.

Journal Pre-proof

Journal Pre-proof

- At OCP – 300 mV, almost 100% of the current density comes from the cathodic reactions (mostly H^+ reduction) while the overall polarization resistance is dominated by R_{p,H_2O} , which is two orders of magnitude smaller than R_{p,H^+} and three orders of magnitude smaller than $R_{p,Fe}$. Therefore, the current density carries information predominantly about H^+ reduction, while the overall polarization resistance carries information predominantly about H_2O reduction: polarization admittance of H_2O reduction is 98.7% of the overall polarization admittance.

3.3. Comparisons with the experimental EIS data

We will now examine if the conclusions drawn above about the dominant reactions at different potentials, based on estimated polarization resistance is consistent with EIS measurements conducted at those same potentials. In Figure 8, if we first look at the spectra collected at the potential OCP + 50 mV and at the OCP, we see that the diameter of the high frequency loop increases, meaning that the charge transfer resistance value increases, i.e. the rate of that reaction decreases at more negative potentials. This confirms that in this potential range, the impedance of the anodic reaction is dominant and is the one being detected by the model in Figure 6 and Figure 7. Moving on to even more negative potentials, ie. OCP – 50 mV, the same trend continues, i.e. the diameter of the high frequency loop i.e. the charge transfer resistance keeps on increasing. This confirms that in this range of potentials, the impedance of the anodic reaction remains dominant, even at OCP – 50 mV where 69.7% of the measured impedance is estimated to come from the anodic reaction (Figure 7), while most of the measured current density (84.8%) is related to the cathodic reaction (Figure 5). We can also observe in Figure 8, that the EIS curves collected at the OCP + 50 mV, at the OCP and at the OCP – 50 mV look quite similar: a depressed semi-circle with an inductive loop at low frequencies that carry information mostly

Journal Pre-proof

about the anodic reaction – oxidation of iron, which dominates the measured impedance in this potential range, as shown above. It has been argued in some previous studies that the high frequency capacitive loop is related to the double layer capacitance followed by a low frequency inductive loop representing the relaxation of $Fe(I)_{ads} \equiv FeOH_{ads}$ as an intermediate species in iron dissolution reaction [3–5,21]

In Figure 9, we had added the spectrum collected at OCP – 100 mV which indicates some of the same trend: an increase in the overall impedance with the decreasing potential. This is consistent with the analysis above, where we concluded that about half of the measured impedance at this potential comes from the anodic reaction, even if it is 100 mV more negative than the OCP. However, the key difference is the absence of the inductive loop, which was associated with the anodic reaction. This is related to the fact that the measured impedance at OCP – 100 mV is influenced by the cathodic reactions as much as the anodic reaction, making it difficult to observe the inductive loop at low frequencies.

In Figure 10, the spectrum collected at OCP – 150 mV is compared to the one obtained at OCP – 100 mV, where we can see a profound change in the shape of the spectra. According to the analysis above, at OCP – 150 mV the measured impedance is dominated by the cathodic reaction – H^+ reduction, being almost entirely under limiting current density control. This is reflected in Figure 10, where this behavior which is consistent with an existence of a so-called Warburg impedance at this potential, indicates the influence of the limiting current density in the low frequency range.

Almost the same behavior is seen at OCP – 200 mV and OCP – 250 mV (Figure 11) where the overall impedance is predominantly influenced by the same cathodic reactions – reduction of H^+ and H_2O, with the former being under limiting current density control and the latter being under

charge transfer control. According to Figure 7, as the potential becomes more negative, the impedance associated with the reduction and H_2O becomes dominant, and being under charge transfer control, we would expect the shape of the spectrum to change. While this is difficult to discern from spectra collected at OCP – 200 mV and OCP – 250 mV, it becomes clear when comparing with a spectrum collected at OCP – 300 mV. There, the measured impedance is significantly smaller, the shape of the curve is quite different with at least two-time constants, all suggesting a new reaction dominating the impedance in this potential range. This is consistent with the analysis presented in Figure 6. It is interesting to note that the H_2O reduction reaction is not clearly discernable in this potential range by just looking at the potentiodynamic sweeps presented in Figure 4. To identify it clearly, it would take approximately another 100 mV of polarization in the more negative direction, yet it dominates the impedance spectrum at this potential.

The values of the charge transfer resistance and polarization resistance as estimated from the impedance spectra (Figure 8 - Figure 11) are compared to polarization resistance calculated from the model fitted to the potentiodynamic sweep curves (Figure 6) and are presented in Table 3. The charge transfer resistance and the polarization resistance were determined by a simple visual inspection of the provided Nyquist plots, without resorting to equivalent circuit analysis and fitting algorithms. Charge transfer resistance is the resistance related to pure charge transfer current density. In other words, when the change in current density is only related to the change in potential, as shown in Equation (18).

$$R_{ct} = \left(\frac{\Delta V}{\Delta i}\right)_{C_i(0),\theta_i} \qquad (18)$$

For H^+ reduction, the polarization resistance is the combination of charge transfer and mass transfer resistances. For iron oxidation, the polarization resistance is associated with the charge transfer resistance and the adsorption kinetics of FeOH on the metal surface. In the vicinity of the corrosion potential, the overall polarization resistance can be represented mostly by the anodic and cathodic polarization resistances in parallel to each other. Reliable estimation of the polarization resistance was possible only for spectra collected at the most positive potentials and the most negative potentials. The spectra collected in the mid-range of potentials, which are strongly influenced by the H^+ reduction reaction, which is under limiting current density control, were not able to provide an accurate estimation of the polarization resistance. Overall, a reasonable agreement is observed which reinforces the validity of the methodology and the interpretations presented above.

4. Conclusion

- A new methodology based on modeling potentiodynamic sweeps has been developed to estimate the dominant electrochemical reaction(s) contributing to the impedance measured by EIS at any potential. This model can help to design experiments by selecting DC potentials in EIS measurements which can best elucidate the behavior of reactions of interest.
- At various potentials, the relative contributions of different reactions to the measured impedance in EIS measurements are not always analogous to their contributions to the measured current density. For example, in the case presented above related to corrosion of mild steel in a CO_2 solution, at a potential 50 mV more negative than the open circuit potential, the dominant reaction contributing to the measured current density is due to the cathodic reaction (H^+ reduction) while the dominant reaction contributing to the measured impedance is the anodic reaction (Fe oxidation).

Declaration of Competing Interest

The author declare that they have no known competing financial interests or personal relationships that could have appeared to influence the work reported in this paper.

Credit authorship contribution statement

Negar Moradighadi: Conceptualization, Investigation, Formal analysis, Writing - original draft. **Srdjan Nesic:** Supervision, Conceptualization, Formal analysis, Writing - review and editing. **Bernard Tribollet:** Supervision, Writing - review and editing.

Acknowledgments

The author would like to acknowledge the financial support from the following companies: Anadarko, Baker Hughes, BP, Chevron, Clariant Corporation, CNOOC, ConocoPhillips, DNV GL, ExxonMobil, M-I SWACO (Schlumberger), Multi-Chem (Halliburton), Occidental Oil Company, Pioneer Natural Resources, Saudi Aramco, Shell Global Solutions, SINOPEC (China Petroleum) and Total.

Appendix A. Nomenclature

C_i	Concentration of species i / mol m^{-3}
D_i	Diffusion coefficient of species i / m^2 s^{-1}
δ_d	Diffusion layer thickness / m
δ_r	Reaction layer thickness / m
η	Over potential / V
F	Faraday constant / C mol^{-1}
i_j	Current density of reaction j / A m^{-2}

Journal Pre-proof

$i_{0,j}$	Exchange current density of reaction j / A m^{-2}
$i_{ch,j}$	Charge transfer controlled current density of rection j / A m^{-2}
$i_{lim,j}$	Limiting current density of reaction j / A m^{-2}
$k_{rds,Fe}$	Rate constant of rate determining step of iron dissolution reaction
k_{f,hy,CO_2}	Rate constant of forward CO_2 hydration reaction / s^{-1}
k_{b,hy,CO_2}	Rate constant of backward CO_2 hydration reaction / s^{-1}
K_{hy,CO_2}	Equilibrium constant of CO_2 hydration reaction
p_i	Partial pressure of species i / bar
ν	Kinematic viscosity / m^2 s^{-1}
R	Universal gas constant / J K^{-1} mol^{-1}
$R_{ct,j}$	Charge transfer resistance of reaction j / ohm cm^2
$R_{p,j}$	Polarization resistance of reaction j / ohm cm^2
T	Temperature / K
V	Electrode potential / V
ω	Angular velocity / rad s^{-1}
θ_i	Surface coverage of species i
Z	Impedance / ohm cm^2
Z'	Real part of impedance / ohm cm^2
Z''	Imaginary part of impedance / ohm cm^2

References

[1] M.E. Orazem, B. Tribollet, Electrochemical Impedance Spectroscopy, 2nd ed., John Wiley & Sons, Inc., Hoboken, NJ, 2017.

Journal Pre-proof

[2] A. Lasia, Electrochemical Impedance Spectroscopy and its Applications, Springer-Verlag, New York, 2014. https://doi.org/10.1007/978-1-4614-8933-7.

[3] M. Keddam, O.R. Mattos, H. Takenouti, Reaction Model for Iron Dissolution Studied by Electrode Impedance: I . Experimental Results and Reaction Model, J. Electrochem. Soc. 128 (1981) 257. https://doi.org/10.1149/1.2127401.

[4] M. Keddam, O.R. Mattos, H. Takenouti, Reaction Model for Iron Dissolution Studied by Electrode Impedance: II . Determination of the Reaction Model, J. Electrochem. Soc. 128 (1981) 266. https://doi.org/10.1149/1.2127402.

[5] T. das Chagas Almeida, M.C.E. Bandeira, R.M. Moreira, O.R. Mattos, New insights on the role of CO_2 in the mechanism of carbon steel corrosion, Corrosion Science. 120 (2017) 239–250. https://doi.org/10.1016/j.corsci.2017.02.016.

[6] G. Baril, G. Galicia, C. Deslouis, N. Pébère, B. Tribollet, V. Vivier, An Impedance Investigation of the Mechanism of Pure Magnesium Corrosion in Sodium Sulfate Solutions, J. Electrochem. Soc. 154 (2006) C108.

[7] S. Amand, M. Musiani, M.E. Orazem, N. Pébère, B. Tribollet, V. Vivier, Constant-phase-element behavior caused by inhomogeneous water uptake in anti-corrosion coatings, Electrochimica Acta. 87 (2013) 693–700. https://doi.org/10.1016/j.electacta.2012.09.061.

[8] M. Musiani, M.E. Orazem, N. Pébère, B. Tribollet, V. Vivier, Determination of resistivity profiles in anti-corrosion coatings from constant-phase-element parameters, Progress in Organic Coatings. 77 (2014) 2076–2083.

[9] I.A.J. Gordon, S. Grugeon, H. Takenouti, B. Tribollet, M. Armand, C. Davoisne, A. Débart, S. Laruelle, Electrochemical Impedance Spectroscopy response study of a commercial graphite-based negative electrode for Li-ion batteries as function of the cell state of charge

Journal Pre-proof

and ageing, Electrochimica Acta. 223 (2017) 63–73. https://doi.org/10.1016/j.electacta.2016.12.013.

[10] Z. He, F. Mansfeld, Exploring the use of electrochemical impedance spectroscopy (EIS) in microbial fuel cell studies, Energy & Environmental Science. 2 (2009) 215–219.

[11] S.K. Roy, M.E. Orazem, B. Tribollet, Interpretation of Low-Frequency Inductive Loops in PEM Fuel Cells, J. Electrochem. Soc. 154 (2007) B1378. https://doi.org/10.1149/1.2789377.

[12] S.S. Zhang, K. Xu, T.R. Jow, EIS study on the formation of solid electrolyte interface in Li-ion battery, Electrochimica Acta. 51 (2006) 1636–1640.

[13] IMPEDANCE | Definition of IMPEDANCE by Oxford Dictionary on Lexico.com, Lexico Dictionaries | English. (n.d.). https://www.lexico.com/definition/impedance.

[14] A. Kahyarian, S. Nesic, A New Narrative for CO_2 Corrosion of Mild Steel, Journal of The Electrochemical Society. 166 (2019) C3048–C3063. https://doi.org/10.1149/2.0071911jes.

[15] J.O. Bockris, D. Drazic, A.R. Despic, The electrode kinetics of the deposition and dissolution of iron, Electrochimica Acta. 4 (1961) 325–361. https://doi.org/10.1016/0013-4686(61)80026-1.

[16] S. Nesic, J. Postlethwaite, S. Olsen, An Electrochemical Model for Prediction of Corrosion of Mild Steel in Aqueous Carbon Dioxide Solutions, CORROSION. 52 (1996) 280–294. https://doi.org/10.5006/1.3293640.

[17] A. Kahyarian, M. Achour, S. Nesic, 34 - Mathematical modeling of uniform CO_2 corrosion, in: A.M. El-Sherik (Ed.), Trends in Oil and Gas Corrosion Research and Technologies, Woodhead Publishing, Boston, 2017: pp. 805–849. https://doi.org/10.1016/B978-0-08-101105-8.00034-6.

Journal Pre-proof

[18] A.J. Bard, L.R. Faulkner, Electrochemical Methods: Fundamentals and Applications, 2nd ed., John Wiley & Sons, Inc., 2001.

[19] V.G. Levich, Physicochemical Hydrodynamics, Prentice-Hall, Englewood Cliffs, N.J, 1969.

[20] M.D.D. Ayagou, M. Tran, B. Tribollet, J. Kittel, E. Sutter, N. Ferrando, C. Mendibide, C. Duret-Thual, Electrochemical impedance spectroscopy of iron corrosion in H 2 S solutions, Electrochimica Acta. 282 (2018) 775.

[21] I. Epelboin, M. Keddam, Faradaic Impedances: Diffusion Impedance and Reaction Impedance, J. Electrochem. Soc. 117 (970) 1052. https://doi.org/10.1149/1.2407718.

Journal Pre-proof

Figures

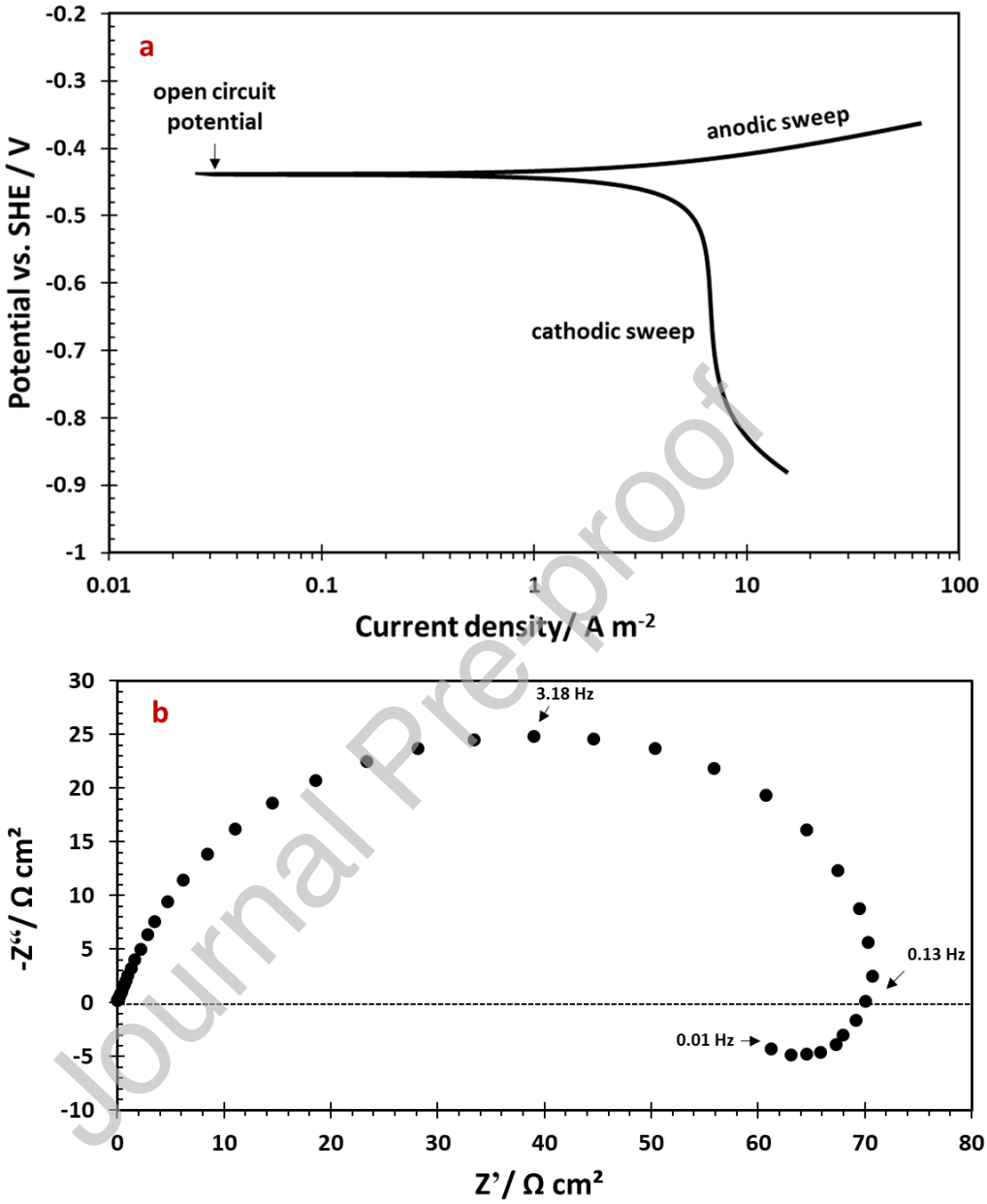

Figure 1. Corrosion of X65 mild steel RDE @ 2000 rpm, 0.1 M NaCl aqueous solution sparged with 1 bar CO_2, pH 4.0, 30 ^{o}C; a) steady state potentiodynamic polarization sweeps; b) electrochemical impedance spectrum conducted at the open circuit potential (OCP) shown as a Nyquist plot.

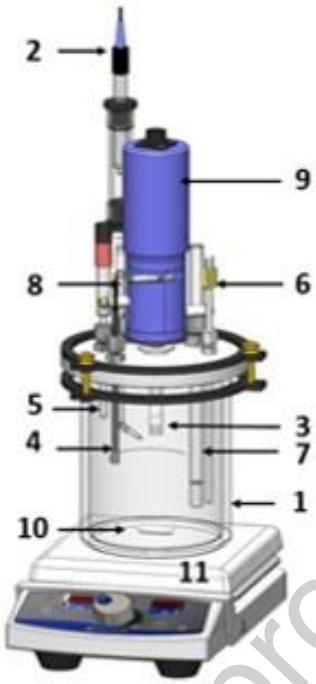

Figure 2. The experimental apparatus: (1) 1 L glass cell; (2) reference electrode (Ag/AgCl); (3) rotating-disk working electrode (X65 mild steel); (4) counter electrode (graphite rod) ; (5) pH probe; (6) thermocouple; (7) gas inlet; (8) gas outlet; (9) motor; (10) magnetic stir bar; and (11) hot plate stirrer. Drawing courtesy of Cody Shafer, OU, ICMT.

Journal Pre-proof

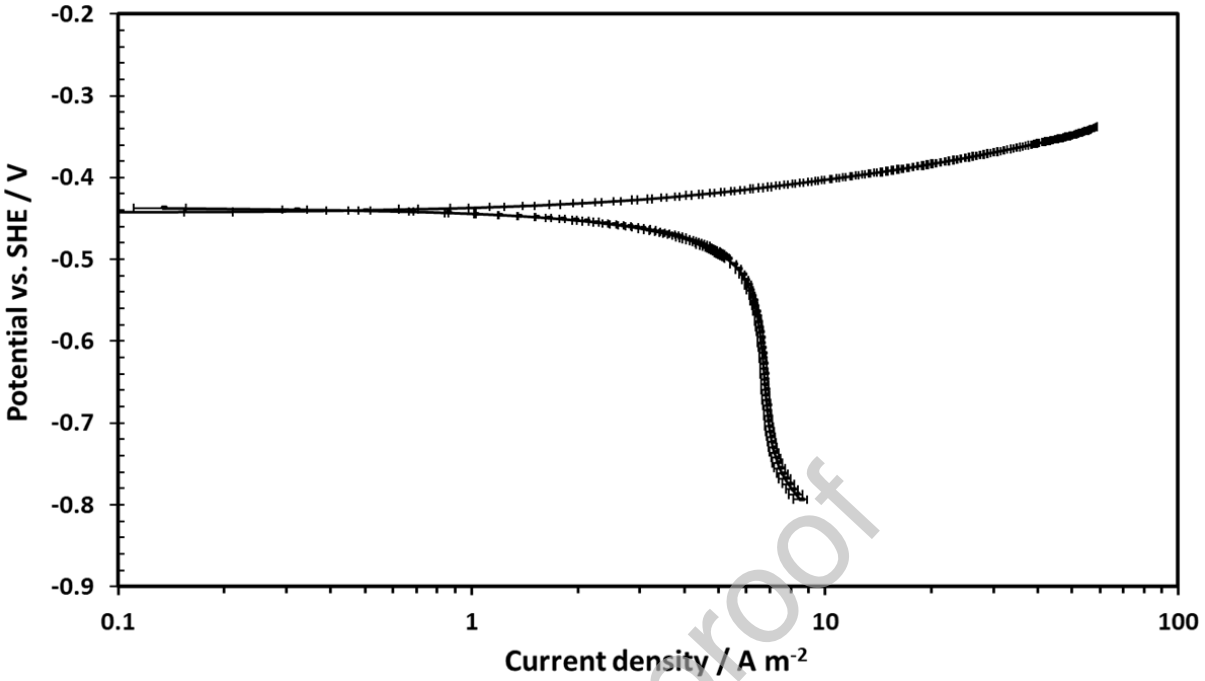

Figure 3. Steady state polarization sweep curve, measured using a sweep rate of 0.125 mV s^{-1}, on X65 mild steel RDE at 2000 rpm, corroding in an aqueous solution at pH 4.0, 30 ^{o}C, saturated at 1 bar CO_2, with 0.1 M NaCl supporting electrolyte. Error bars represent minimum and maximum current densities calculated in duplicated experiments.

Journal Pre-proof

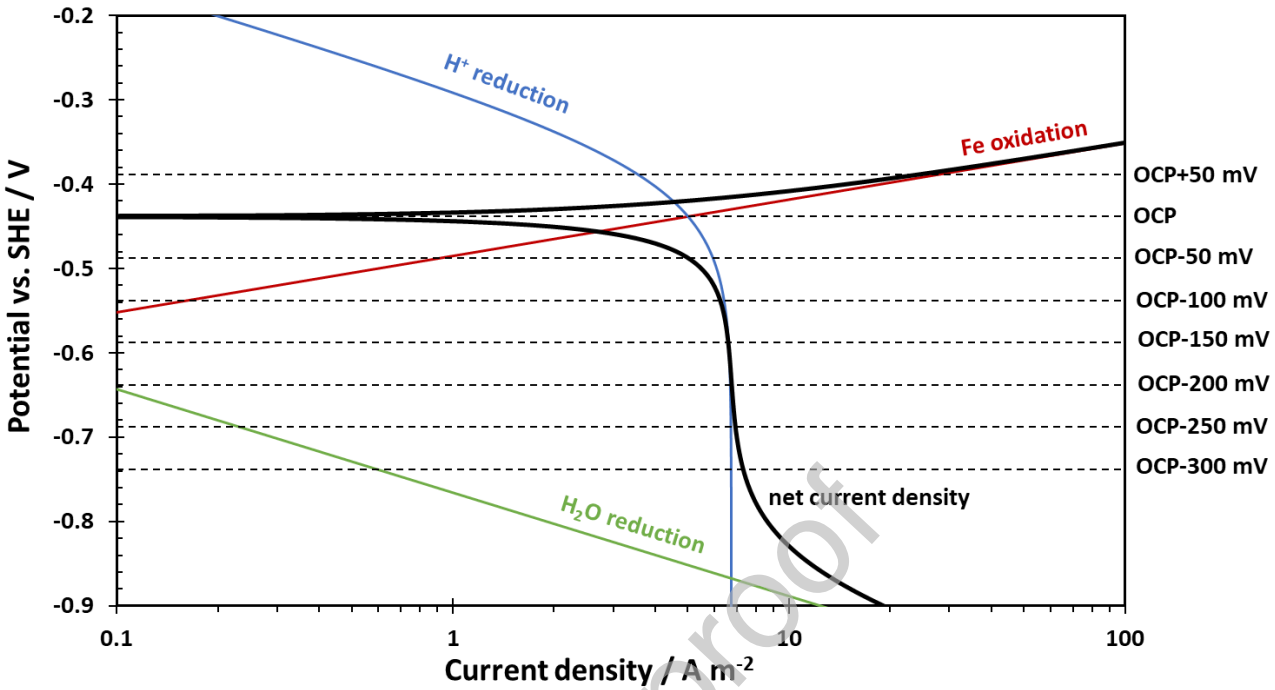

Figure 4. Experimental and modeled steady state potentiodynamic sweep of individual reactions underlying the overall potentiodynamic sweep shown in Figure 3. Modeling parameters: mild steel RDE at 2000 rpm, pH 4.0, 30 ^{o}C, aqueous solution saturated at 1 bar CO_2, with 0.1 M NaCl supporting electrolyte.

Journal Pre-proof

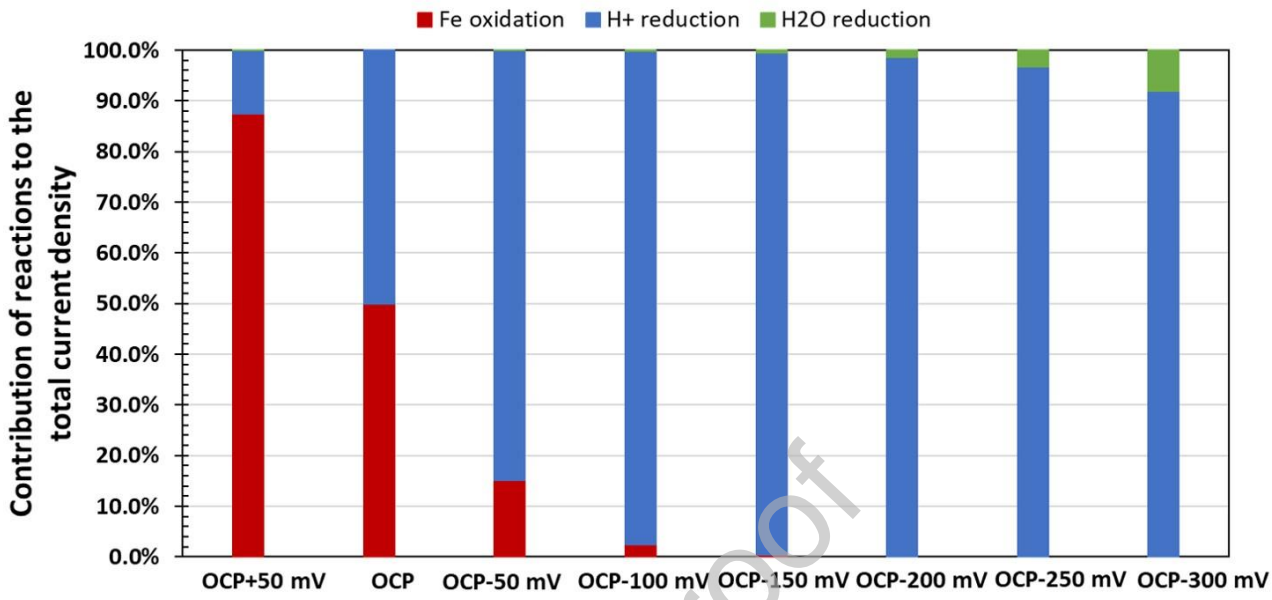

Figure 5. Contribution of each reaction (H^+ reduction, Fe oxidation and H_2O reduction) to the total current density, based on Figure 4. Modeling parameters: X65 mild steel RDE, 2000 rpm, pH 4.0, 30 ^oC, aqueous solution saturated at 1 bar CO_2, and with 0.1 M NaCl supporting electrolyte.

Journal Pre-proof

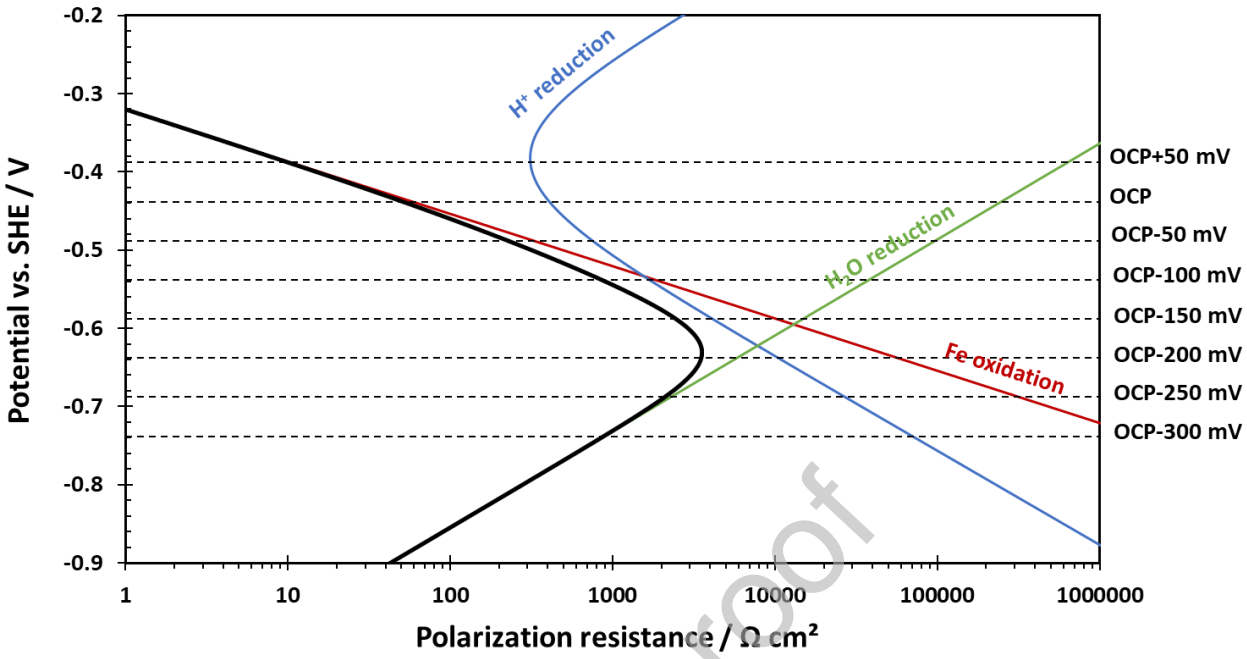

Figure 6. Modeled polarization resistance of H^+ reduction, Fe oxidation, H_2O reduction and overall polarization resistance, derived from the modeled potentiodynamic sweeps shown in Figure 4. Modeling parameters: X65 mild steel RDE, 2000 rpm, pH 4.0, 30 ^oC, aqueous solution saturated at 1 bar CO_2, and with 0.1 M NaCl supporting electrolyte.

Journal Pre-proof

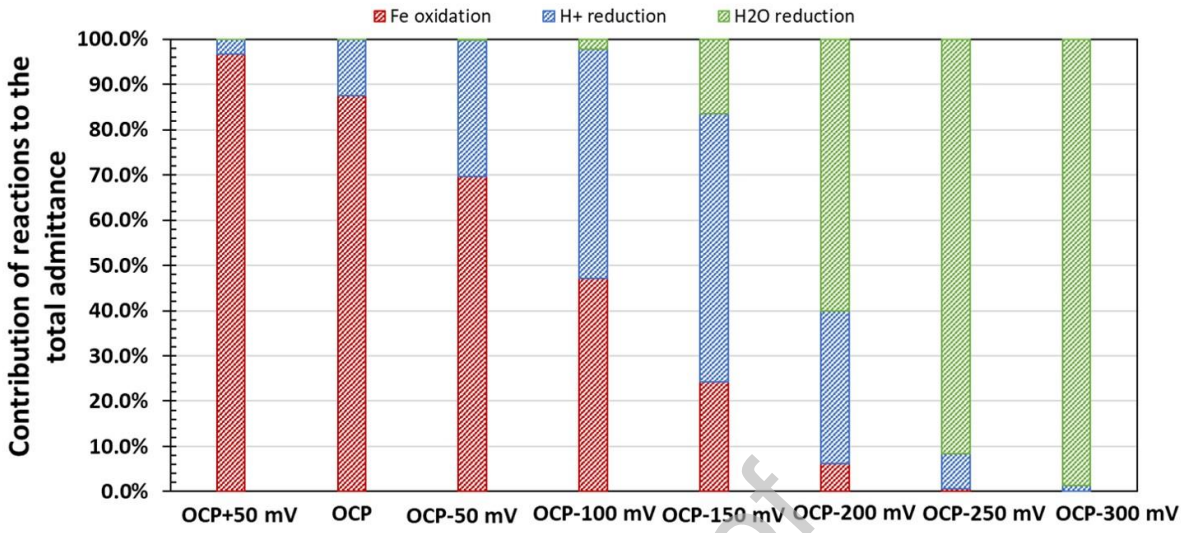

Figure 7. Contribution of individual reaction (H^+ reduction, Fe oxidation and H_2O reduction) to the total admittance, based on Figure 6. Modeling parameters: X65 mild steel RDE, 2000 rpm, pH 4.0, 30 ^oC, aqueous solution saturated at 1 bar CO_2, and with 0.1 M NaCl supporting electrolyte.

Journal Pre-proof

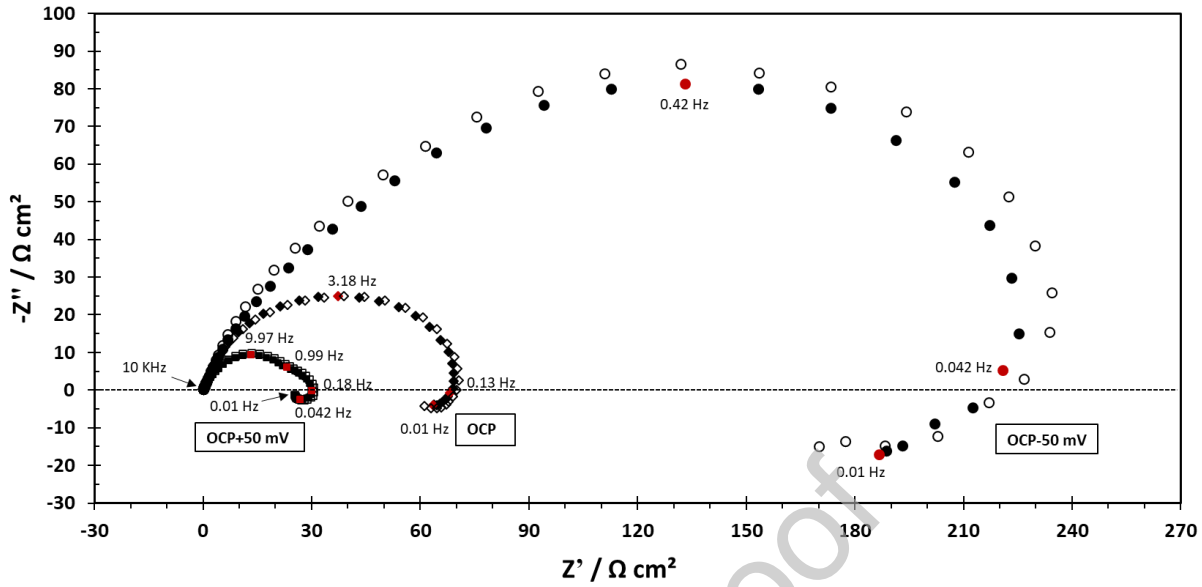

Figure 8. Nyquist plot at OCP + 50 mV, OCP, and OCP – 50 mV. Experimental parameters: X65 mild steel RDE, 2000 rpm, pH 4.0, 30 ^{o}C, aqueous solution saturated at 1 bar CO_2, 0.1 M NaCl supporting electrolyte and frequency range from 10,000 - 0.01 Hz. Nyquist plots having the same shaped markers represents duplicated experiments.

Journal Pre-proof

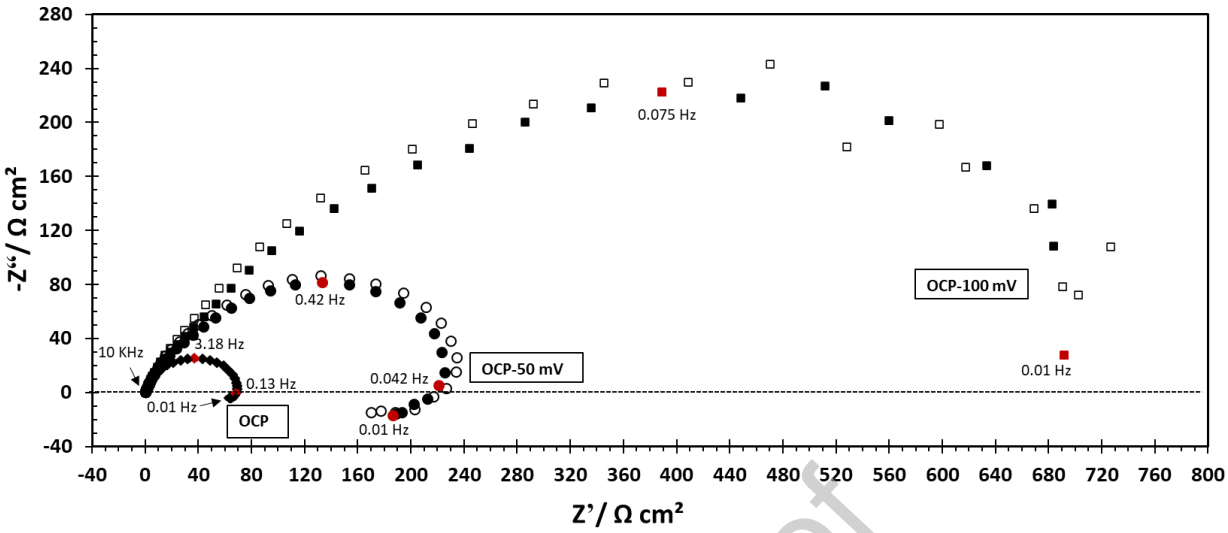

Figure 9. Nyquist plot at different OCP, OCP – 50 mV and OCP – 100 mV. Experimental parameters: X65 mild steel RDE, 2000 rpm, pH 4.0, 30 °C, aqueous solution saturated at 1 bar CO_2, 0.1 M NaCl supporting electrolyte and frequency range from 10,000 - 0.01 Hz. Nyquist plots having the same shaped markers represents duplicated experiments.

Journal Pre-proof

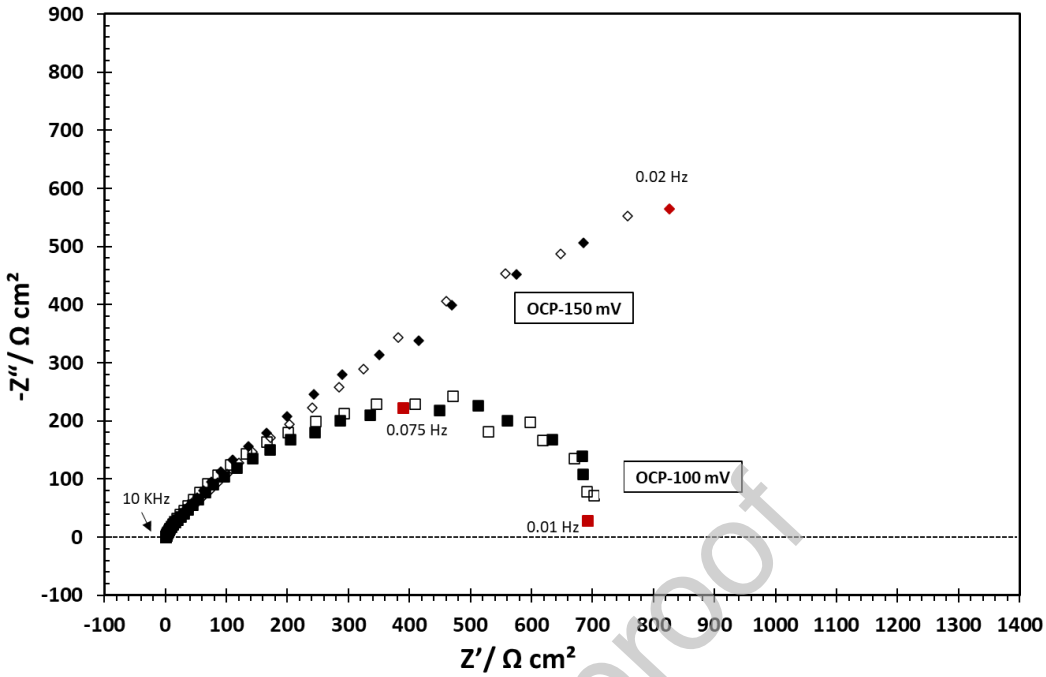

Figure 10. Nyquist plot at different OCP – 100 mV and OCP – 150 mV. Experimental parameters: X65 mild steel RDE, 2000 rpm, pH 4.0, 30 ^{o}C, aqueous solution saturated at 1 bar CO_2, 0.1 M NaCl supporting electrolyte and frequency range from 10,000 - 0.01 Hz. Nyquist plots having the same shaped markers represents duplicated experiments.

Journal Pre-proof

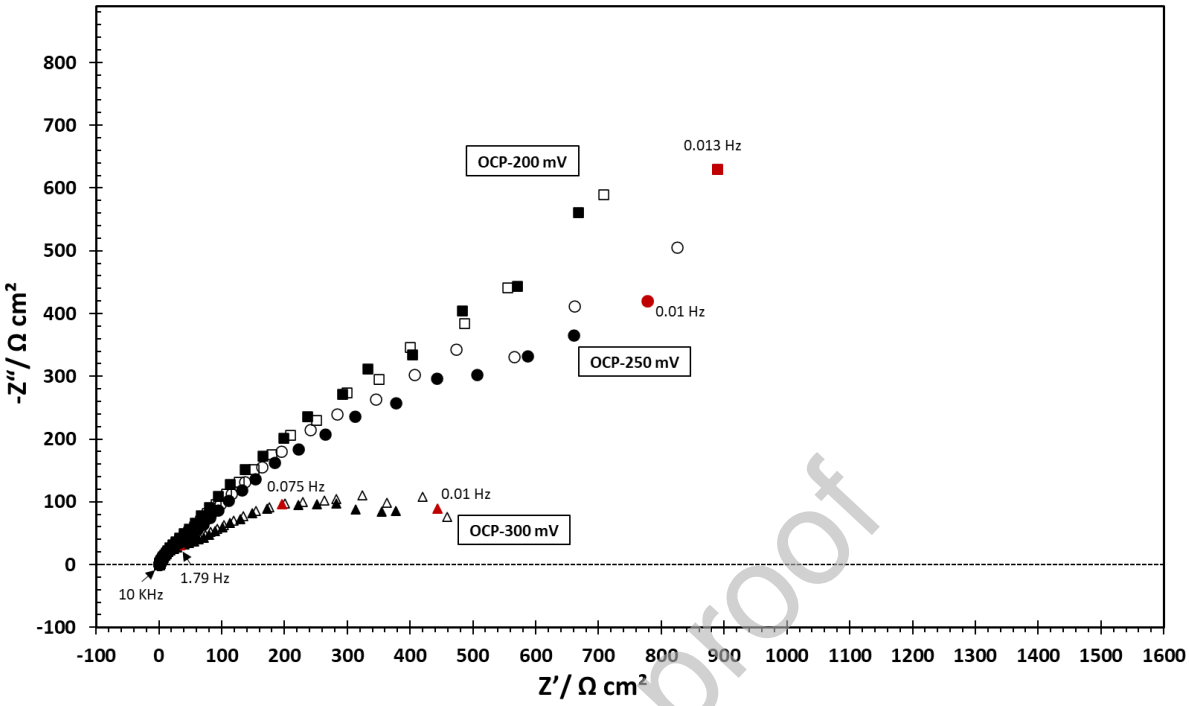

Figure 11. Nyquist plot at different OCP – 200 mV, OCP – 250 mV and OCP – 300 mV. Experimental parameters: X65 mild steel RDE, 2000 rpm, pH 4.0, 30 ^{o}C, aqueous solution saturated at 1 bar CO_2, 0.1 M NaCl supporting electrolyte and frequency range from 10,000 - 0.01 Hz. Nyquist plots having the same shaped markers represents duplicated experiments.

Journal Pre-proof

Tables:

Table 1

Chemical composition of API 5L X65

Element	C	Nb	Cr	Ni	Mn	S	P	Ti	Al	Fe
Composition /wt%	0.05	0.03	0.15	0.38	1.51	<0.001	0.004	0.01	0.033	Balance

Journal Pre-proof

Table 2

Experimental conditions

Parameters	**Values**
Test apparatus	Rotating disk electrode Three-electrode glass cell
Sparge gas	pCO_2 = 1 bar
Temperature	30±0.5 ^oC
pH	4.00±0.01
Supporting electrolyte	0.1 M NaCl
Rotation rate	2000 rpm
Electrode material	API 5L X65
Parameters of the EIS scans:	
Frequency	from 10000 to 0.01 Hz
AC potential	10 mV rms.
DC potential	OCP (– 435±1 mV vs SHE)
	OCP – 50 mV
	OCP – 100 mV
	OCP – 150 mV
	OCP – 200 mV
	OCP – 250 mV
	OCP – 300 mV
	OCP + 50 mV

Journal Pre-proof

Journal Pre-proof

Table 3

Comparison of charge transfer resistance estimated from EIS measurements (Figure 8-Figure 11) with the polarization resistance calculated from the model fitted to the potentiodynamic sweeps (Figure 6). Modeling and experimental parameters: mild steel RDE at 2000 rpm, pH 4.0, 30^{o}C, aqueous solution saturated at 1 bar CO_2, with 0.1 M NaCl supporting electrolyte.

	OCP +50 mV	OCP	OCP –50 mV	OCP –100 mV	OCP –150 mV	OCP –200 mV	OCP –250 mV	OCP –300 mV
R_{ct} from EIS experiments / Ω cm^2	30±1	70±1	223±3	719±6	125±5	113±7	96±2	85±5
R_p from EIS experiments / Ω cm^2	25±1	57±2	148±5	719±6	cannot be reliably determined	cannot be reliably determined	cannot be reliably determined	520±20
R_p from model potentiodynamic sweep / Ω cm^2	10	51	225	851	2447	3518	2772	883

Journal Pre-proof